

Polymer Solar Cells Based on the Copolymers of Naphtho[1,2-*c*:5,6-*c'*]bis(1,2,5-thiadiazole) and Alkoxyphenyl Substituted Benzodithiophene with High Open-Circuit Voltages

Liqian Liu, Guichuan Zhang, Baitian He, and Fei Huang*

Institute of Polymer Optoelectronic Materials and Devices, State Key Laboratory of Luminescent Materials and Devices, South China University of Technology, Guangzhou, Guangdong 510640, China

Two novel naphtho[1,2-*c*:5,6-*c'*]bis(1,2,5-thiadiazole) and alkoxyphenyl substituted benzodithiophene based copolymers were developed as the donor materials for polymer solar cells. The resulting copolymers exhibit broad absorption bands in the range of 500–800 nm in thin films and deep highest occupied molecular orbital energy levels of –5.39 eV and –5.36 eV, respectively. The best device performance was achieved by P1, with an open-circuit voltage of 0.85 V, a short-circuit current density of 8.65 mA•cm⁻², a fill factor of 37.8%, and a power conversion efficiency of 2.78%.

Keywords polymer solar cells, donor materials, alkoxyphenyl substituted, naphtho[1,2-*c*:5,6-*c'*]bis(1,2,5-thiadiazole)

Introduction

The growing interests in polymer solar cells (PSCs) are due to their unique advantages such as low-cost manufacturing and easy processability over large-area size via printing and roll-to-roll coating technologies, and compatibility with flexible substrates and materials, which enable them for potential applications in low-cost photovoltaic systems.^[1–6] The most common architecture to build PSCs is the bulk heterojunction (BHJ) structure prepared by mixing electron-rich donor polymers and electron-deficient fullerenes, because high power conversion efficiencies (PCEs) can be achieved by this method.^[7–24] Generally, there are three important parameters that governed the PCEs of PSCs—short current density (J_{sc}), open circuit voltage (V_{oc}), and fill factor (FF). To improve the J_{sc} value of the resulting PSCs, the narrow band gap donor polymers have been extensively developed due to their good coverage of absorption in the solar spectrum. However, the excessively narrowing band gaps of donor polymers may have a negative effect on the overall device performance of the resulting polymers, since the decreased band gap often means the increased highest occupied molecular orbital (HOMO) energy level and decreased lowest unoccupied molecular orbital (LUMO) energy level. When considering that V_{oc} is related to the difference between the HOMO energy level of the donor and the LUMO energy level of the acceptor, the high HOMO levels for

donor polymers are not desired to attain high V_{oc} . Therefore, to obtain a good device performance, an ideal low band gap polymer should make a trade-off between its open circuit voltage and band gap.

Recently, many kinds of copolymers have been successfully developed and showed excellent photovoltaic properties. Among them, benzodithiophene (BDT) and naphtho[1,2-*c*:5,6-*c'*]bis(1,2,5-thiadiazole) (NT) based polymer (*i.e.* PBDT-DTNT) exhibited promising photovoltaic properties.^[25–27] For example, in a conventional device structure, PBDT-DTNT exhibited a much improved PCE of 6.0% compared to the analogous polymer with BT as an acceptor.^[25] By using a conjugated polyelectrolyte interfacial layer within an inverted solar cell device, the PCE of PBDT-DTNT was further enhanced to 8.4%.^[28] The exciting PCE of this polymer was mainly due to its broad solid absorption spectrum and highly planar conjugated backbone, which are favorable for high J_{sc} . However, the relatively low V_{oc} value limits the further improvement of its photovoltaic properties. If the V_{oc} could be enhanced without sacrificing much of the other properties, one could expect a better device performance of BDT-NT based polymers.

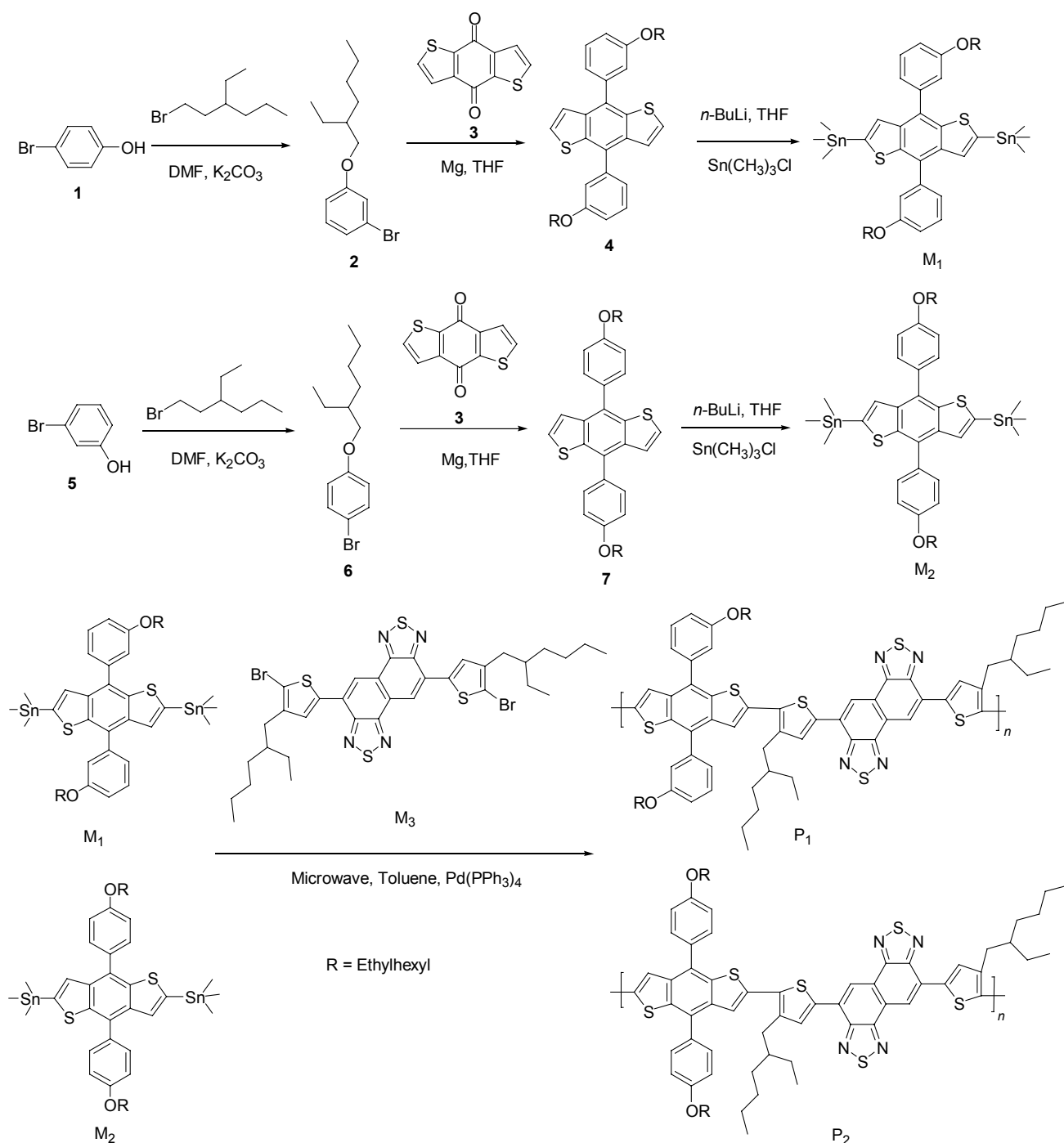
In this work, we designed and synthesized two novel polymer donor materials based on BDT and NT units (Scheme 1, P1 and P2). Compared to their analogous polymer PBDT-DTNT, the alkylthienyl substituted BDT was replaced by alkoxyphenyl substituted BDT (BDTP) to lower the HOMO energy levels of the

* E-mail: msfhuang@scut.edu.cn

Received March 31, 2015; accepted May 13, 2015; published online June 10, 2015.

Supporting information for this article is available on the WWW under <http://dx.doi.org/10.1002/cjoc.201500265> or from the author.

Scheme 1 Synthetic routes of monomers and polymers



resulting polymer.^[29-31] As a result, P1 and P2 exhibited deep HOMO energy levels of -5.39 and -5.36 eV, respectively. Photovoltaic properties of P1 were investigated. In a conventional device structure, a V_{oc} of as high as 0.92 V was realized. The best device performance was obtained in an inverted device structure and a PCE value of 2.78% with a V_{oc} of 0.85 V were achieved.

Experimental

The synthetic routes of monomers and polymers are shown in Scheme 1. The polymers are synthesized by

microwave-assisted Stille polycondensation reaction with good yield. Detailed synthetic procedure can be found in the Experimental Section. P1 shows good solubility in chlorinated solvents such as chlorobenzene and *o*-dichlorobenzene (*o*-DCB). However, P2 shows very poor solubility in common solvents and can only be partially dissolved in hot *o*-DCB and trichlorobenzene. The poor solubility can be ascribed to both the axial symmetry and centro symmetry structure of M2, which leads to a very strong molecular packing interaction of the resulting polymers. The number average molecular weight (M_n) and polydispersity index (PDI) of polymer P1 are

14.2 K and 2.3, respectively, which are estimated by high temperature gel permeation chromatography (GPC) using trichlorobenzene as the solvent and polystyrene with narrow molecular weight distribution as a standard. The thermogravimetric analysis (TGA) results show that P1 and P2 have good thermal stability with an onset of decomposition temperature of *ca.* 350 °C (See Figure S1 in Supporting Information, SI).

Results and Discussion

UV-vis absorption spectra of the polymer in *o*-DCB and as a solid film were shown in Figure 1a. P1 and P2 show three absorption bands in the range 300–800 nm both in solution and in the solid film. The absorption maxima of P1 and P2 are both located at *ca.* 580 nm in solution, and P2 shows an obvious shoulder peak at *ca.* 635 nm, which illustrates that parts of polymer molecules of P2 start to aggregate in solution. The strong packing ability of P2 corresponds to its poor solubility. In thin solid films, both P1 and P2 exhibited considerably more significant red-shifted absorbance compared with solution data, which is a common feature of linear donor-acceptor conjugated polymers. This phenomenon is caused by the increased polymer chain aggregation in the solid state. The absorption maxima of P1 and P2 are located at *ca.* 612 and 660 nm, respectively. The absorption edges (λ_{edge}) of polymer film of P1 and P2 are located at *ca.* 755 and 793 nm, corresponding to optical band gaps ($E_{\text{g}}^{\text{opt}}$) of 1.64 and 1.56 eV, respectively.

Cyclic voltammetry (CV) measurements are performed in order to evaluate the electrochemical properties and molecular energy levels of the resulting polymers. Graphite, platinum wire, and Ag/AgCl were used as the working electrode, counter electrode, and reference electrode, respectively. All measurements are carried out in tetrabutyl ammonium hexafluorophosphate (Bu_4NPF_6) solution (0.1 mol/L in acetonitrile) at a scan rate of $50 \text{ mV}\cdot\text{s}^{-1}$ under inert atmosphere. As shown by the cyclic voltammograms in Figure 1b, the electrochemical oxidation onset potentials (E_{ox}) of P1 and P2 referred to ferrocene/ferrocenium (Fc/Fc^+) were 0.59 and 0.56 V, respectively, which correspond to the HOMO energy levels of -5.39 and -5.36 eV according to the equation of $\text{HOMO} = -e(E_{\text{ox}} + 4.80)$ (eV). Compared to PBDT-DTNT with alkylthienyl substituted BDT as donor unit with an HOMO energy of -5.19 eV, both of the resulting polymers show a deeper HOMO energy level. The deeper HOMO energy level demonstrates that by changing chemical structure of side chains of conjugated polymers, electrochemical property of conjugated polymers could be effectively tuned. The LUMO energy levels are calculated from the difference between the HOMO energy levels and the optical band gap energies according to the equation: $\text{LUMO} = (\text{HOMO} + E_{\text{g}}^{\text{opt}})$ eV, and the corresponding LUMO energy levels were -3.75 and -3.80 eV for P1 and P2, respectively.

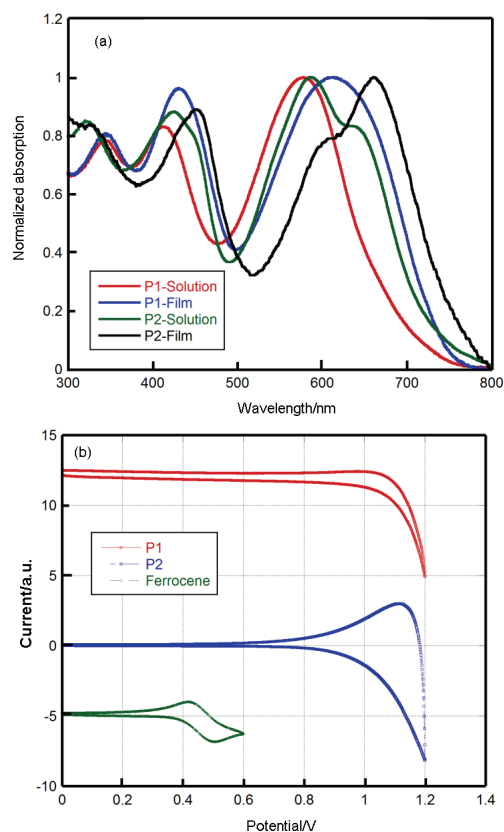


Figure 1 (a) The absorption spectra of the polymer in *o*-DCB and in solid film. (b) Cyclic voltammogram of polymer film on a glassy carbon electrode measured in $0.1 \text{ mol}\cdot\text{L}^{-1}$ Bu_4NPF_6 acetonitrile solution at a scan rate of $50 \text{ mV}\cdot\text{s}^{-1}$.

Table 1 Photovoltaic performance of devices measured under simulated light (AM 1.5G, $100 \text{ mW}\cdot\text{cm}^{-2}$)

Device structure	D/A ration	PCE/%	$J_{\text{sc}}/(\text{mA}\cdot\text{cm}^{-2})$	V_{oc}/V	FF/%
Conventional structure	1 : 1	0.69	2.78	0.94	26.36
	1 : 2	1.30	4.81	0.92	29.48
	1 : 3	1.11	4.42	0.86	29.24
Inverted structure	1 : 1	0.66	2.97	0.89	24.97
	1 : 2	1.19	4.44	0.90	29.80
	1 : 2 (2% DIO)	2.78	8.65	0.85	37.80
	1 : 3	1.09	4.51	0.85	28.38

PSC devices were fabricated and characterized to investigate the photovoltaic properties of the resulting polymers. Firstly, the conventional device structure of ITO/PEDOT:PSS/polymers:PC₇₁BM/PFN/Al was used. The conjugated polyelectrolytes were used to improve charge injection from electrodes into organic active layers.^[32,33] The BHJ photoactive materials were dissolved in hot *o*-DCB with stirring overnight before spin-coating on substrate. P1 exhibited a very good film forming capability. However, P2 can not form uniform thin films through spin-coating due to its poor solubility. As a result, P2 based devices exhibited a very poor device performance. Therefore, only device with P1/PC₇₁BM

blend as active layer was further carefully investigated. PSC devices with different D/A ratios (P1/PC₇₁BM, w/w) were fabricated to optimize the D/A ratio of the blend. Table 1 showed the photovoltaic parameters of the resulting devices under the illumination of AM 1.5G (100 mW/cm²) with different D/A ratios (1 : 1, 1 : 2 and 1 : 3). It is clear that the optimal D/A ratio of the blend is 1 : 2, and a PCE of 1.30% was obtained with a V_{oc} of 0.92 V, a J_{sc} of 4.81 mA/cm², and an FF of 29.48%. Compared with PBDT-DTNT with the same device structure (V_{oc} =0.80 V), a much improved V_{oc} was obtained in P1 based devices.

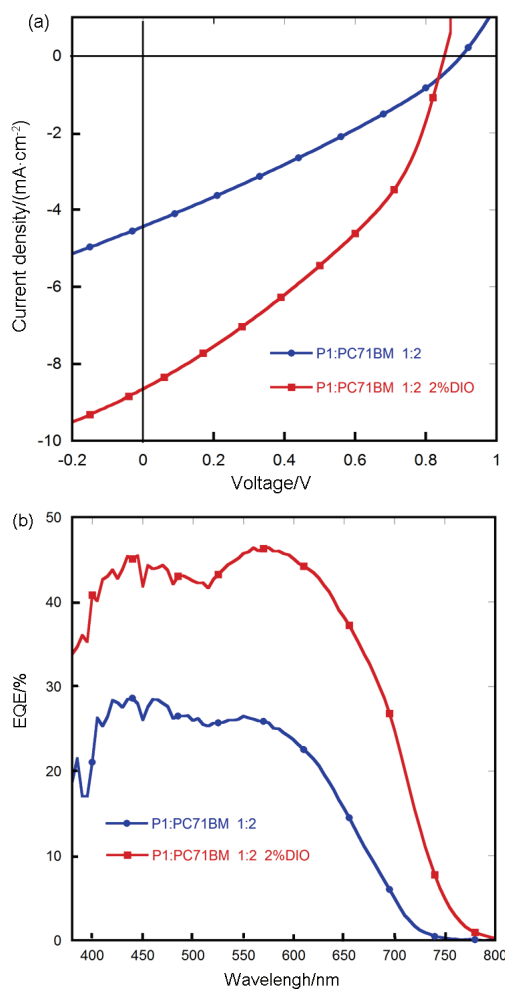


Figure 2 (a) J - V curves and (b) EQE spectra of devices with the configuration: ITO/PFN/active-layer/MoO₃/Al.

The inverted PSCs with the structure of ITO/PFN/P1:PC₇₁BM/MoO₃/Al was also fabricated to investigate the photovoltaic properties of P1 because inverted devices typically demonstrate better ambient stability compared to conventional devices.^[34,35] It was found that P1 showed similar PCEs compared to that in conventional structure when using different D/A ratios. To further improve the photovoltaic performance of the device, 1,8-diiodooctane (DIO) was added to the solutions prior to the spin-coating process. The photovoltaic performance of the resulting device can be significantly

improved by adding a small amount of DIO (2%) as the additive. Figure 2 showed the J - V curve and EQE of solar cells based on the P1/PC₇₁BM blend films without and with 2% DIO as the additive. Table 1 summarized the photovoltaic parameters of the resulting devices. Compared to the devices processed without additive, the devices processed with DIO showed a slightly lower V_{oc} , a slightly higher FF, and a remarkably improved J_{sc} . Under optimal processing condition, the PCE of device based on P1 was 2.78% with a V_{oc} of 0.85 V, a J_{sc} of 8.65 mA/cm² and an FF of 37.8%. The nanoscale morphology of blend film was tested by using atomic force microscopy (AFM) and phase graphs are shown in Figure 3. The surface roughness measured from the topograph image was 0.93 and 2.63 for P1 without and with DIO, respectively. The film without DIO exhibits smoother surface morphology. However, the film with DIO shows much obvious nanoscale phase separation, which is favorable for charge separation and transport.

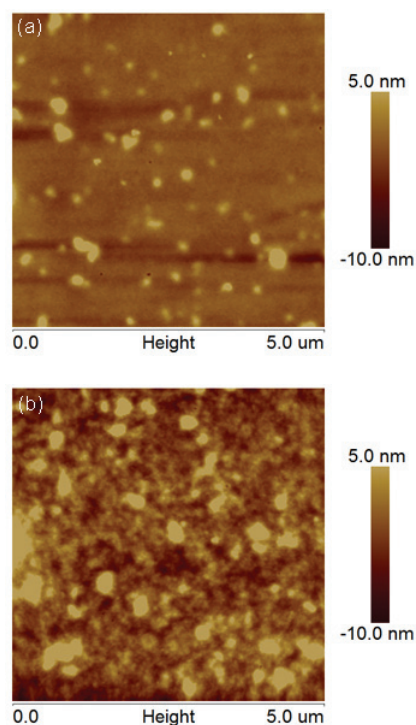


Figure 3 AFM images: (a) P1 film without DIO; (b) P1 film with DIO. All images are 5 μm × 5 μm.

To investigate the influence of the DIO on the device performance, hole mobility of the resultant polymers was examined by using the space charge limited current (SCLC) model with the device configuration of ITO/poly(3,4-ethylenedioxythiophene):poly(styrenesulfonate) (PEDOT:PSS)/active-layer/MoO₃/Al. The mobilities were determined by fitting the dark currents to the model of a single carrier SCLC, which is described by the equation $J = (9/8)\epsilon_0\epsilon_r\mu_h(V^2/d^3)$, where J is the current, μ_h is the zero-field mobility, ϵ_0 is the permittivity of free space, ϵ_r is the relative permittivity of the material, d is the thickness of the polymer layer, and V is the

effective voltage. The effective voltage was obtained by subtracting the built-in voltage (V_{bi}) and the voltage drop (V_s) from the series resistance of the substrate from the applied voltage (V_{app}), $V = V_{app} - V_{bi} - V_s$. The mobilities were extracted by modeling the dark currents in the SCLC region and calculated from the slope of the $J^{1/2}$ - V curves as shown in Figure 4. It was found that the hole mobility of active layer was hugely improved when adding DIO. The hole mobilities of active layer before and after adding DIO were 2.40×10^{-5} and 1.81×10^{-4} $\text{cm}^2 \cdot \text{V}^{-1} \cdot \text{s}^{-1}$, respectively. The remarkably improved J_{sc} could be ascribed to the higher hole mobility.

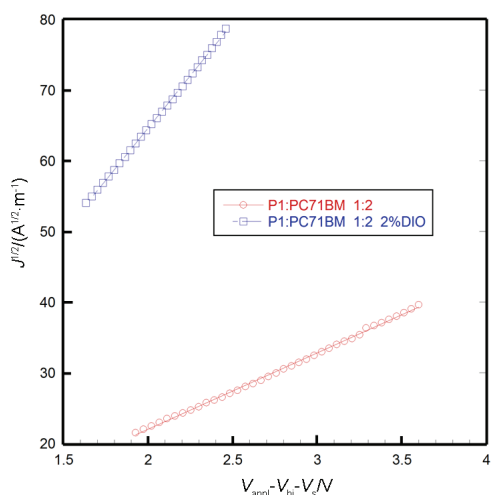


Figure 4 $J^{1/2}$ - V characteristics of devices with the configuration: ITO/PEDOT:PSS/active-layer/MoO₃/Al. The solid lines represent the fit curves.

Conclusions

In conclusion, we designed and synthesized two novel polymer donor materials based on BDTP and NT units. Compared to PBDT-DTNT with alkylthienyl substituted BDT as donor unit, both of the novel synthesized polymers show a much deeper HOMO energy level. As a result, solar cell devices based on polymer P1 obtained a V_{oc} as high as 0.92 V, much higher than that of PBDT-DTNT with a V_{oc} of 0.80 V in identical device structure. Under optimal condition, PSCs based on P1:PC₇₁BM (1 : 1, *w/w*) with 2% DIO showed a PCE of 2.78% with a V_{oc} of 0.85 V, a J_{sc} of 8.65 mA/cm^2 , and an FF of 37.8%, under the illumination of AM 1.5G, 100 mW/cm^2 . Our results demonstrated that by changing the chemical structure of side chains of conjugated polymers, the V_{oc} of polymers could be effectively tuned.

Experimental Section

Materials

Benzo[1,2-*b*:4,5-*b'*]dithiophene-4,8-dione (**3**), 4,8-bis(3-ethylhexyloxy-1-phenyl)-benzo[1,2-*b*:4,5-*b'*]dithiophene (**4**), 3,7-(di(2-bromo-3-(2-ethylhexyl)-5-thienyl)-naphtho[1,2-*c*:5,6-*c'*]-bis[1,2,5]thiadiazole) (**M3**)

were prepared according to the reported procedures.^[31,36] All chemicals and reagents were purchased from commercial sources (Aldrich, Acros, and Alfa Aesar) and used without further purification unless stated otherwise.

2,6-Bis(trimethyltin)-4,8-bis(3-ethylhexyloxy-1-phenyl)-benzo[1,2-*b*:4,5-*b'*]dithiophene (M1) A solution of compound **4** (1.2 g 2 mmol) in dry THF (30 mL) was deoxygenated with argon for 30 min, and then 2.4 mol/L *n*-butyllithium solution in *n*-hexane (3.33 mL, 8 mmol) was added dropwise at 0 °C. Then the solution was allowed to warm up to 40 °C for 2 h, and 1.0 mol/L trimethyltin chloride solution in THF (10 mL, 10 mmol) was added. Then the mixture was poured into water and extracted with dichloromethane. The organic phase was evaporated, and the residue was recrystallized from 20 mL methanol to afford the pale yellow solid (1.2 g, 65%). ¹H NMR (600 MHz, CDCl₃) δ : 7.48 (t, $J=7.79$ Hz, 2H), 7.41 (s, 2H), 7.31 (d, $J=7.21$ Hz, 2H), 7.25 (s, 2H), 7.03 (dd, $J=8.32, 1.8$ Hz, 2H), 3.90 (d, $J=6.06$ Hz, 4H), 1.80–1.77 (m, 2H), 1.56–1.38 (m, 16H), 0.99–0.93 (m, 12H), 0.35 (s, 18H); ¹³C NMR (125 MHz, CDCl₃) δ : 159.29, 141.97, 141.65, 140.79, 136.51, 130.41, 129.33, 128.51, 121.19, 114.88, 114.43, 70.35, 39.02, 30.20, 28.70, 23.57, 22.70, 13.72, 10.76, –8.75.

4,8-Bis(4-ethylhexyloxy-1-phenyl)-benzo[1,2-*b*:4,5-*b'*]dithiophene (7) 1-Bromo-4-(2-ethylhexyloxy)benzene (17.1 g, 60 mmol) was added dropwise to magnesium turnings (1.5 g, 62.5 mmol) in anhydrous THF (35 mL) under the protection of argon. During the process, I₂ (10 mg) was added as catalyst in the reaction. The solution was refluxed for 3 h then was cooled down. The solution was added slowly to benzo[1,2-*b*:4,5-*b'*]dithiophene-4,8-dione (4.4 g, 20 mmol) dispersed in 40 mL THF. SnCl₂ (25 g) was dissolved in 10% aqueous HCl (40 mL) and then added dropwise. The solution was stirred for another 1 h at 50 °C. After cooling to room temperature, the mixture was poured into water and extracted with dichloromethane, the organic extraction was washed successively with water and sodium bicarbonate solution twice and the combined organic phase was dried over magnesium sulfate and evaporated to afford the crude product. The crude product was purified on a silica gel column, eluting with pure hexane. Light yellow crystals were obtained (3.6 g, 30% yield). ¹H NMR (600 Hz, CDCl₃) δ : 7.63 (d, $J=8.69$ Hz, 4H), 7.36–7.33 (m, 4H), 7.09 (d, $J=8.63$ Hz, 4H), 3.96–3.94 (m, 4H), 1.81–1.77 (m, 2H), 1.56–1.38 (m, 16H), 0.99–0.93 (m, 12H); ¹³C NMR (125 MHz, CDCl₃) δ : 159.26, 138.30, 136.25, 131.41, 130.51, 130.02, 127.01, 123.11, 114.75, 70.56, 39.50, 30.62, 29.17, 23.96, 23.12, 14.16, 11.22.

2,6-Bis(trimethyltin)-4,8-bis(4-ethylhexyloxy-1-phenyl)-benzo[1,2-*b*:4,5-*b'*]dithiophene (M2) A solution of compound **7** (1.2 g, 2 mmol) in dry THF (30 mL) was deoxygenated with argon for 30 min, and then 2.4 mol/L *n*-butyllithium solution in *n*-hexane (3.33 mL,

8 mmol) was added dropwise at 0 °C. Then the solution was allowed to warm up to 40 °C for 2 h, and 1.0 mol/L trimethyltin chloride solution in THF (10 mL, 10 mmol) was added. Then the mixture was poured into water and extracted with dichloromethane. The organic phase was evaporated, and the residue was recrystallized from 20 mL methanol to afford the white solid (1.3 g, 70%). ¹H NMR (600 MHz, CDCl₃) δ: 7.65 (d, *J*=8.59 Hz, 4H), 7.38 (s, 2H), 7.11 (d, *J*=8.62 Hz, 4H), 3.96 (d, *J*=5.50 Hz, 4H), 1.82–1.78 (m, 2H), 1.60–1.36 (m, 16H), 1.00–0.93 (m, 12H), 0.35 (s, 18H); ¹³C NMR (125 MHz, CDCl₃) δ: 159.07, 142.60, 141.63, 137.08, 132.07, 130.87, 130.59, 128.46, 114.66, 70.50, 39.55, 30.64, 29.18, 23.97, 23.12, 14.16, 11.23, –8.34.

Synthesis of P1

Compound M1 (92.4 mg, 0.10 mmol), compound M3 (79.1 mg, 0.10 mmol), Pd(PPh₃)₄ (5 mg), and toluene (5 mL) were added to a 35 mL reaction vial. The vial was purged with argon and subsequently sealed. The vial was heated in a microwave reactor at 180 °C for 45 min. Then the reaction mixture was cooled to ambient temperature and precipitated into methanol. The solid was collected by filtration. After drying in the vacuum drying oven, the crude product was purified by Soxhlet extraction with methanol, acetone and hexane and to remove oligomers and residual catalyst. Finally, the polymer P1 was obtained as a dark-green solid (80.3 mg, 79% yield).

Synthesis of P2

The polymerization procedure for compound M2 (92.4 mg, 0.10 mmol) and compound M3 (79.1 mg, 0.10 mmol) was the same as that of P1. P2 was obtained as a dark-green solid (91.5 mg, 90%).

Instruments and characterization

The NMR data was collected on a Bruker AVANCE Digital 600 MHz NMR workstation. Gel permeation chromatography (150 °C in 1,2,4-trichlorobenzene) was performed on a Polymer Laboratories PL220 Chromatograph with linear polystyrene as references. UV-vis absorption spectra were measured using an HP 8453 spectrophotometer. The solutions that were used for the UV-visible spectroscopy measurements were dissolved in *o*-DCB, and the films were dropcoated from the *o*-DCB solution onto a quartz substrate. Thermogravimetric analyses were carried out with a Netzsch TG 209 under N₂ flow at a heating rate of 10 °C·min⁻¹. The electrochemical cyclic voltammetry was conducted on CHI 600D electrochemical workstation at a scan rate of 50 mV·s⁻¹.

Fabrication and characterization of polymer solar cells

Conventional device structure: ITO coated glass substrates were cleaned by sonication in detergent, deionized water, acetone and isopropyl alcohol and dried

in a nitrogen stream, followed by an oxygen plasma treatment. To fabricate photovoltaic devices, a hole transport thin layer (*ca.* 40 nm) of PEDOT:PSS (Baytron PVP Al 4083, filtered at 0.45 μm) was spin coated on the precleaned ITO-coated glass substrates at 5000 r/min and baked at 140 °C for 10 min under ambient conditions. The substrates were then transferred into an argon-filled glove box. Subsequently, the polymer: PC₇₁BM active layer (*ca.* 100 nm) was spin-coated on the top of PEDOT:PSS layer from a homogeneous blend solution. A thin layer of PFN (5 nm) was spin-coated from methanol solution on the top of active layer. To complete device fabrication, the substrates were pumped down to a high vacuum (1 × 10⁻⁶ Torr), and aluminum (100 nm) was thermally evaporated through shadow masks. The effective devices area was measured to be 0.16 cm².

Inverted device structure: ITO glass substrates were used as the cathode in the polymer solar cells. The ITO coated glass substrates were cleaned by sonication in detergent, deionized water, acetone, and isopropyl alcohol and dried in a nitrogen stream. Then PFN (0.5 mg·mL⁻¹) was spin-cast from *V*(methanol) : *V*(acetic acid) = 100 : 1 onto the ITO substrate to form a 5 nm thin film. The bulk heterojunction composite with thickness of 100 nm was then spin coated on PFN layer from *o*-DCB solution of polymer (5 mg·mL⁻¹) and PC₇₁BM. After that, about 10 nm molybdenum oxide (MoO₃) was thermally deposited on top of the active layer through a shadow mask in a vacuum chamber with an evaporation rate of 0.1 Å·s⁻¹ under a vacuum of *ca.* 3 × 10⁻⁴ Pa. The effective area of a device was 0.16 cm² as determined by the shadow mask used during deposition of Al electrode.

Power conversion efficiencies (PCEs) were measured under an AM 1.5 G XES-40S1 150W AAA Class Solar Simulator. The power of the sun simulation was calibrated before the testing using a standard silicon solar cell, giving a value of 100 mW·cm⁻² during the test. The current density-voltage (*J*-*V*) characteristics were recorded with a Keithley 2400 Source Measure Unit. The spectral response was measured with a commercial photo modulation spectroscopic setup (Oriel). A calibrated Si photodiode was used to determine the photosensitivity. The external quantum efficiencies of the inverted PSCs were measured with a commercial photomodulation spectroscopic setup (DSR100UV-B) including a xenon lamp, an optical chopper, a monochromator, and a lock-in amplifier operated by a PC computer (Zolix Instruments), and a calibrated Si photodiode was used as a standard.

Acknowledgement

The work was financially supported by the Ministry of Science and Technology (No. 2014CB643501), the Natural Science Foundation of China (Nos. 21125419, 51361165301) and Guangdong Natural Science Founda-

tion (No. S2012030006232).

References

- [1] Yu, G.; Gao, J.; Hummelen, J. C.; Wudl, F.; Heeger, A. J. *Science* **1995**, *270*, 1789.
- [2] Dennler, G.; Scharber, M. C.; Brabec, C. J. *Adv. Mater.* **2009**, *21*, 1323.
- [3] Lungenschmied, C.; Dennler, G.; Neugebauer, H.; Sariciftci, S. N.; Glatthaar, M.; Meyer, T.; Meyer, A. *Sol. Energy Mater. Sol. Cells* **2007**, *91*, 379.
- [4] Li, Y. F. *Acc. Chem. Res.* **2012**, *45*, 723.
- [5] Krebs, F. C. *Sol. Energy Mater. Sol. Cells* **2009**, *93*, 394.
- [6] Dennler, G.; Scharber, M. C.; Brabec, C. J. *Adv. Mater.* **2009**, *21*, 1323.
- [7] Thompson, B. C.; Frechet, J. M. *Angew. Chem., Int. Ed.* **2008**, *47*, 58.
- [8] Liu, Y.; Zhao, J.; Li, Z.; Mu, C.; Ma, W.; Hu, H.; Jiang, K.; Lin, H.; Ade, H.; Yan, H. *Nat. Commun.* **2014**, *5*, 5293.
- [9] He, Z.; Zhong, C.; Su, S.; Xu, M.; Wu, H.; Cao, Y. *Nat. Photonics* **2012**, *6*, 591.
- [10] Hu, X.; Yi, C.; Wang, M.; Hsu, C.-H.; Liu, S.; Zhang, K.; Zhong, C.; Huang, F.; Gong, X.; Cao, Y. *Adv. Energy Mater.* **2014**, *4*, 1400378.
- [11] Subbiah, J.; Purushothaman, B.; Chen, M.; Qin, T.; Gao, M.; Vak, D.; Scholes, F. H.; Chen, X.; Watkins, S. E.; Wilson, G. J.; Holmes, A. B.; Wong, W. W.; Jones, D. J. *Adv. Mater.* **2015**, *27*, 702.
- [12] Cui, C.; Wong, W.; Li, Y. *Energy Environ. Sci.* **2014**, *7*, 2276.
- [13] Zhao, G.; He, Y.; Peng, B.; Li, Y. *Chin. J. Chem.* **2012**, *30*, 19.
- [14] Wang, J.; Ye, H.; Li, H.; Mei, C.; Ling, J.; Li, W.; Shen, Z. *Chin. J. Chem.* **2013**, *31*, 1367.
- [15] Chen, L.; Shen, X.; Chen, Y. *Chin. J. Chem.* **2012**, *30*, 2219.
- [16] Chen, S.; Tang, C.; Yin, Z.; Ma, Y.; Cai, D.; Ganeshan, D.; Zheng, Q. *Chin. J. Chem.* **2013**, *31*, 1409.
- [17] Deng, P.; Xiong, J.; Li, S.; Wu, Y.; Yang, J.; Zhang, Q. *Chin. J. Chem.* **2014**, *32*, 521.
- [18] Duan, C.; Wang, C.; Liu, S.; Huang, F.; Choy, C. H. W.; Cao, Y. *Sci. China Chem.* **2011**, *54*, 685.
- [19] Huang, L.; Yang, D.; Gao, Q.; Liu, Y.; Lu, S.; Zhang, J.; Li, C. *Chin. J. Chem.* **2013**, *31*, 1385.
- [20] Li, W.; Li, Q.; Liu, S.; Duan, C.; Ying, L.; Huang, F.; Cao, Y. *Sci. China Chem.* **2015**, *58*, 257.
- [21] Liu, L.; van Bavel, S.; Wen, S.; Yang, X.; Loos, J. *Chin. J. Chem.* **2013**, *31*, 731.
- [22] Wang, J.; Ye, H.; Li, H.; Mei, C.; Ling, J.; Li, W.; Shen, Z. *Chin. J. Chem.* **2013**, *31*, 1367.
- [23] Xiao, B.; Cheng, X.; Zhao, B.; Wu, H. *Chin. J. Chem.* **2013**, *31*, 1423.
- [24] Zhang, S.; Ye, L.; Zhao, W.; Yang, B.; Wang, Q.; Hou, J. *Sci. China Chem.* **2015**, *58*, 248.
- [25] Wang, M.; Hu, X.; Liu, P.; Li, W.; Gong, X.; Huang, F.; Cao, Y. *J. Am. Chem. Soc.* **2011**, *133*, 9638.
- [26] Osaka, I.; Kakara, T.; Takemura, N.; Koganezawa, T.; Takimiya, K. *J. Am. Chem. Soc.* **2013**, *135*, 8834.
- [27] Liu, L. Q.; Zhang, G. C.; Liu, P.; Zhang, J.; Dong, S.; Wang, M.; Ma, Y. G.; Yip, H. L.; Huang, F. *Chem.-Asian J.* **2014**, *9*, 2104.
- [28] Yang, T.; Wang, M.; Duan, C.; Hu, X.; Huang, L.; Peng, J.; Huang, F.; Gong, X. *Energy Environ. Sci.* **2012**, *5*, 8208.
- [29] Dou, L.; Gao, J.; Richard, E.; You, J.; Chen, C. C.; Cha, K. C.; He, Y.; Li, G.; Yang, Y. *J. Am. Chem. Soc.* **2012**, *134*, 10071.
- [30] Zhang, M.; Gu, Y.; Guo, X.; Liu, F.; Zhang, S.; Huo, L.; Russell, T. P.; Hou, J. *Adv. Mater.* **2013**, *25*, 4944.
- [31] Zhang, M.; Guo, X.; Ma, W.; Zhang, S.; Huo, L.; Ade, H.; Hou, J. *Adv. Mater.* **2014**, *26*, 2089.
- [32] Liu, S.; Zhang, Z.; Chen, D.; Duan, C.; Lu, J.; Zhang, J.; Huang, F.; Su, S.; Chen, J.; Cao, Y. *Sci. China Chem.* **2013**, *56*, 1119.
- [33] Liu, S.; Zhong, C.; Zhang, J.; Duan, C.; Wang, X.; Huang, F. *Sci. China Chem.* **2011**, *54*, 1745.
- [34] Yip, H.-L.; Jen, A. K. Y. *Energy Environ. Sci.* **2012**, *5*, 5994.
- [35] He, Z.; Zhong, C.; Huang, X.; Wong, W. Y.; Wu, H.; Chen, L.; Su, S.; Cao, Y. *Adv. Mater.* **2011**, *23*, 4636.
- [36] Wang, M.; Hu, X.; Liu, L.; Duan, C.; Liu, P.; Ying, L.; Huang, F.; Cao, Y. *Macromolecules* **2013**, *46*, 3950.

(Cheng, F.)